

# Prediction of Extreme Events in Multiscale Simulations of Geophysical Turbulence using Reinforcement Learning

Yifei Guan<sup>1,2</sup>, Lucas Amoudruz<sup>3</sup>, Sergey Litvinov<sup>3</sup>, Karan Jakhar<sup>1,4</sup>, Rambod Mojtani<sup>1</sup>,  
Petros Koumoutsakos<sup>3,†</sup>, and Pedram Hassanzadeh<sup>1,5,†</sup>

<sup>1</sup>Department of Geophysical Sciences, University of Chicago, 5801 S Ellis Avenue, Chicago, 60637 IL, USA

<sup>2</sup>Department of Mechanical Engineering, Union College, 807 Union Street, Schenectady, 12308 NY, USA

<sup>3</sup>Computational Science and Engineering Laboratory, Harvard University, 29 Oxford Street Cambridge, 02138 MA, USA

<sup>4</sup>Department of Mechanical Engineering, Rice University, 6100 Main Street, Houston, 77005 TX, USA

<sup>5</sup>Committee on Computational and Applied Mathematics, University of Chicago, 5747 S Ellis Avenue, Chicago, 60637 IL, USA

<sup>†</sup>Corresponding authors: petros@seas.harvard.edu and pedramh@uchicago.edu

## Abstract

Accurate subgrid-scale closures are essential for weather/climate models, where predicting extreme events is critical. Traditional closures have structural errors, e.g., producing excessive diffusion that dampens extremes. Artificial intelligence has gained attention for closure modeling, but the prediction of extreme events remains challenging. Supervised offline learning needs abundant high-fidelity training data and can lead to instabilities. Online learning algorithms are emerging as an alternative, but reliance on differentiable numerical solvers or scalable optimizers hinders broad use. Here, we introduce scientific multi-agent reinforcement learning (SMARL) to develop closures for canonical prototypes of atmospheric/oceanic turbulence, using only the enstrophy spectrum, estimated from a few high-fidelity samples, as reward. This reward ensures that the model captures the cascades of scales in these simulations. These online-learned closures enable stable simulations, with up to five orders of magnitude fewer degrees of freedom, that reproduce high-fidelity simulation statistics and capturing in particular extremes. We interpret the closures by analyzing the SMARL policy and demonstrate generalization to other flows. The results highlight SMARL as a potent tool for developing closures capable of capturing extremes in atmospheric/oceanic flows, opening new capabilities for effective climate modeling.

## 1 Introduction

Extreme weather events have enormous socioeconomic impacts [1, 2], increasing the demand for the accurate estimates of their statistics, e.g., frequency, especially in a changing climate [3, 4, 5]. However, due to their rarity and complex physics, high-fidelity simulations of these extreme events needs global climate models (GCMs) that are fast, thus of moderate to low resolution, while adequately representing the underlying multi-scale physics of the atmosphere, and more broadly, the Earth system. Practically fast-enough GCMs, which have typical resolutions of  $\mathcal{O}(10) - \mathcal{O}(100)$  km, require sub-grid scale (SGS) closures (parameterizations) for many physical processes [6, 7, 8]. However, traditional physics-based closures have various parametric and structural errors, making them the main source of epistemic uncertainty in climate change predictions

and weather forecasts, especially for extreme events [9, 10, 11, 12]. Artificial intelligence (AI) applications for enhancing efficiency, e.g. through direct emulation of high-resolution simulations from GCMs or other models [13, 14, 15] or rare-event sampling with AI + GCM [16], are emerging. However, these applications are in their early stages, and AI models have been shown to have challenges with the most extreme weather events, particularly those rarer and stronger than events in the training set, the so-called gray swans [17, 16]. Furthermore, even with these approaches, the need for high-fidelity closures for GCMs remains [18].

Recently, there has been great interest in using AI, particularly deep neural networks (DNNs), to develop better closures by learning directly from data. These AI-based approaches can be broadly categorized into two groups: supervised (offline) learning and online learning [12]. In supervised learning, snapshots of high-fidelity data (e.g., from direct numerical simulation (DNS)) are used as reference, then filtered and coarse-grained to extract the SGS terms [19, 20, 21]. The filtered data are then used to train a DNN to learn the mapping between the filtered flow and the SGS terms such as fluxes. Once trained, the DNN is coupled to a low-resolution numerical solver, the large-eddy simulation (LES) hereafter, which represents a practical GCM. Studies with a variety of canonical prototypes of atmospheric and oceanic turbulence have shown the possibility of outperforming classical physics-based closures such as Smagorinsky and Leith models [22, 23, 20, 24, 25]. In particular, it was found that these DNN-based closures not only reproduce the right amount of diffusion, but also capture backscattering, i.e., the forcing of the large-scale flow by the SGS eddies, an important but challenging process for physics-based closures [26, 7].

However, to work accurately, the supervised-learning approach has several major shortcomings: it is data hungry (a significant bottleneck for realistic systems), requires exact SGS terms extracted from high-fidelity data (a non-trivial task), and can lead to unstable LES (with the root cause(s) remaining unclear) [27, 28, 12]. As a result, supervised-learning with DNNs faces significant challenges in scaling up beyond prototypes and to GCMs. More recently, supervised-learning with physics-constrained equation-discovery has shown promises as a data-efficient tool for developing accurate, generalizable, and interpretable closures [29]. However, the LES with these closures is not stable for very low resolutions including those that could be of practical interest in atmosphere and ocean modeling.

Online learning is emerging as a potent alternative to supervised learning, with the closure being learned by a DNN while it is directly coupled to the low-resolution numerical (LES) solver. Here, the goal may not be to match spatially local flow quantities (such as the state’s trajectory or the SGS field), but rather, to match the low-order statistics of the high-fidelity simulations (e.g., DNS) or even (sparse) observations. In climate modeling, these statistics could be key properties of climate variability [30] or kinetic energy spectra of turbulent flows [31, 32]. Finally, online learning can account for the interactions between several closures, a common problem in climate modeling [11] and unaddressed by supervised learning. We distinguish three related approaches to online learning: 1) using a differentiable LES solver/GCM that allows using backpropagation for optimization [33, 34, 35], 2) using derivative-free ensemble-based optimization methods; e.g., ensemble Kalman inversion (EKI) [36, 37, 38, 30, 39, 40], and 3) using reinforcement learning [41, 42, 43, 44]. The first two approaches are actively pursued in the climate community with promising results, including the scale up of approach (1) to realistic weather and climate prediction in Google’s NeuralGCM [45]. However, several major challenges remain. For example, most current GCMs are not differentiable, and a differentiable solver requires a significant change in the modeling and software infrastructure [18]. Approach (2) works with non-differentiable solvers, however, is largely limited to addressing parametric uncertainty but not structural uncertainty [40].

SMARL has improved the parametric and structural uncertainties of closures for LES of 3D homogeneous and wall-bounded turbulent flows [41, 42, 44, 43]. However, its potential for climate modeling applications has remained unexplored. We note that the extension of models for homogeneous and wall-bounded flows to LES of geophysical turbulence and to GCM is not straightforward. In LES of homogeneous turbulent flows [41], the states were based on specific well-known invariants of these flows. Similarly SMARL-based wall models of turbulent flows required knowledge of the law of the wall to determine effective states and actions [43].

In this paper, we introduce the first application of reinforcement learning to closure modeling of geophysical turbulence. As summarized in Fig. 1, we apply SMARL to a canonical prototype: several setups of 2D

turbulence that contain a broad range of scales, structures (jets and vortices), and dynamics, well representing some of the key characteristics of atmospheric and oceanic flows (see Table 1 for details). Details of the approach can be found in Methods. Briefly,

- i We train a SMARL-based closure using low-order statistics. We use global states and targets to train a DNN and learn the flow-dependent coefficient  $c_l$  of a physics-based closure (Leith model) by matching the enstrophy spectrum of the LES+SMARL solver with that of a very short DNS. These few training samples are far too few for DNN-based supervised learning. The LES solver does not need to be differentiable here.
- ii We test the performance of this closure by comparing the kinetic energy spectrum and vorticity probability density function (PDF) of the DNS with LES having 160 to 163, 840 $\times$  spatio-temporally coarser resolution. The LES+SMARL spectrum and PDF match that of the DNS for simulations that are  $\sim 2000\times$  the length of the training dataset. In particular, the PDFs match at the tails, which represent the rare extreme weather events in these prototypes. The LES+SMARL work at resolutions much lower than those required by the recently AI-discovered closure of [46].
- iii We analyze the interpretability of the SMARL-based closures, using Sobol indices to indicate the significance of contributions of the states to the actions. We also show that these closures learn both diffusion and backscattering, with the distribution of  $c_l$  substantially differing from those estimated using dynamic Leith. This shows the ability of this approach in addressing both parametric and structural uncertainty.
- iv We demonstrate successful generalization of the SMARL-based closures on a turbulent flow with 15 $\times$  higher  $Re$  than its training DNS data.

Together, (i)-(iv) demonstrate the promises of SMARL over supervised learning and other online learning approaches.

## 2 Online learning of closures with SMARL

Since the pioneering work of Smagorinsky [47] for the closure modeling of geophysical turbulence, various eddy-viscosity models have been proposed. However, the Smagorinsky [47] and Leith [48] models remain today the most widely used closures. In these models, energy transfer from the resolved to subgrid scales is formulated as non-linear diffusion [49], often with dynamic coefficients that depend on space and time [50, 51]. The parameters of these models are estimated from local constraints, such as the Germano identity of energy transfer in dynamic Smagorinsky (DSmag), and the enstrophy transfer in dynamic Leith (DLeith). The coefficients in Smagorinsky ( $c_s$ ) and Leith ( $c_l$ ) models are used to estimate the turbulence eddy viscosity:  $\nu_e = c_s \Delta^2 |\bar{\mathcal{S}}|$  [52], and  $\nu_e = c_l \Delta^3 |\nabla \bar{\omega}|$  [53, 54], respectively. Using these expressions, the turbulent shear stress, or subgrid stress, has the same form in both models [49, 55, 56]:

$$\tau^{\text{SGS}} = -2\nu_e \sqrt{2\mathcal{S}_{ij}\mathcal{S}_{ij}}, \quad \mathcal{S}_{ij} = \frac{1}{2} \left( \frac{\partial u_i}{\partial x_j} + \frac{\partial u_j}{\partial x_i} \right). \quad (1)$$

In this work, we use SMARL to learn a fully-connected DNN that estimates the Leith coefficient ( $c_l$ ) dynamically (also referred to as RL-Leith) and compare its performance to DLeith and DSmag (we have found RL-Leith and RL-Smag to perform similarly; see the appendix). In the context of the SMARL framework, the state of the system  $s'(t)$  is defined by the enstrophy spectrum  $\hat{Z}(k, t)$  up to the Nyquist wavenumber at LES (or cut-off wavenumber)  $k_c$ . The RL-Leith coefficients are thus expressed as  $c_l(x, y, t) = f_{\text{DNN}}(\hat{Z}(k, t))$ . We place  $n_{A,x} \times n_{A,y}$  agents distributed uniformly on the simulation grid. These agents produce actions that are interpolated onto the computation grid using a polynomial of  $2^{nd}$ -order that preserves the periodicity of the domain. See Fig. 1 and Methods for the details of the SMARL setup, including the reward function (Eq. (4)) and the training procedure.

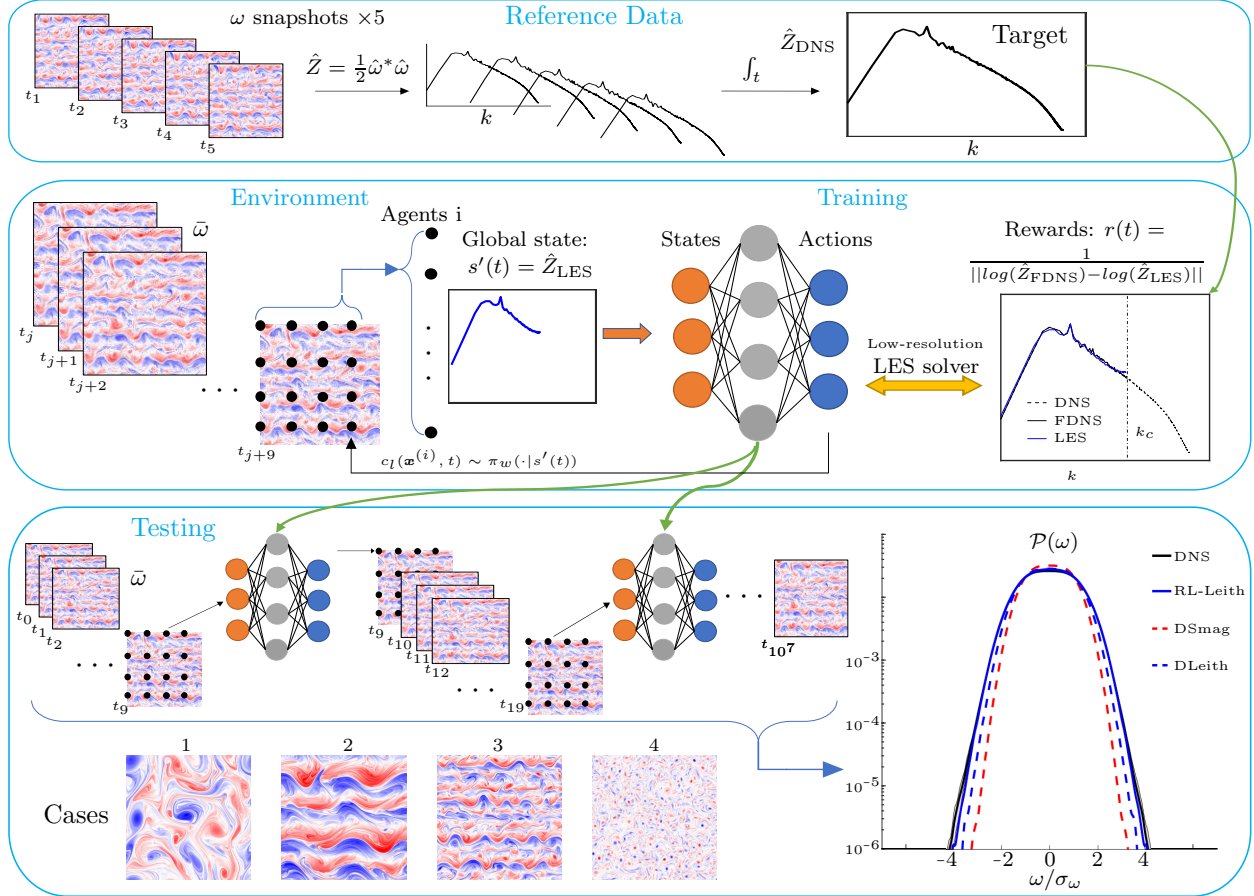


Figure 1: Training of SMARL for SGS closures: (1) reference data consists of 5 samples of a short DNS (Eqs. (2a) and (2b)); (2) online training of agents. The state-action map has input state  $s'(t)$  (spectrum of enstrophy  $\hat{Z}$  up to LES cutoff wavenumber  $k_c$ ) and domain-averaged output action  $c_l(t)$  (coefficient in the closure, Eq. (1)) that maximizes the reward  $r(t)$ . During testing, the policy is coupled to the low-resolution numerical solver to produce a long LES that is  $2000\times$  longer than the DNS training set and  $1000\times$  the training horizon. Performance for extreme events is evaluated in terms of the vorticity PDF  $\mathcal{P}(\omega)$ , against DNS and dynamic physics-based SGS models.

### 3 Results and Discussion

We evaluated the proposed framework in five test cases, described in detail in Section 5.5. These benchmarks are widely used for atmospheric, oceanic, and planetary flows [57, 58, 24, 20, 59, 21]. The simulations correspond to a two-dimensional flow with sinusoidal forced turbulence in a periodic domain. This forcing term generates coherent structures of different scales. In addition, some cases contain a Coriolis force  $\beta$  that represents the rotation of the spherical Earth and generates jet streams. The benchmarks are performed on a range of Reynolds numbers covering different turbulence regimes.

#### 3.1 Prediction of extreme events

We quantify extreme events by estimating the probability density function  $\mathcal{P}(\omega)$  of the vorticity field  $\omega$  over time and space. Positive (cyclonic) and negative (anti-cyclonic)  $\omega$  in this prototype of atmospheric circulation correspond to low- and high-pressure weather systems, whose large amplitudes (tails) drive various types of extreme events [60]. Fig. 2 shows  $\mathcal{P}(\omega)$  computed from cases 1-4 against the prediction performance of RL-Leith, DSmag, and DLeith. In all cases, the RL-Leith model outperforms traditional physics-based dynamic models in terms of matching the DNS PDF. Except for case 4, the RL-Leith PDF matches the DNS within uncertainties, even up at the tails of the distribution, corresponding to low probability or *extreme* events. The lack of extreme events in the DSmag and DLeith predictions is attributed to the excessive diffusion from the positive clipping essential for stability [20]. This is consistent with Fig. 3 showing the excessive interscale enstrophy transfer predicted by DSmag and DLeith for all cases. Other *a-posteriori* analysis, including the turbulent kinetic energy spectra, is included in Section A.

#### 3.2 Enstrophy transfer between scales

A main criterion for a functional eddy-viscosity LES model is the correct prediction of the the total energy/enstrophy transfer between resolved and subgrid scales [49]. Fig. 3 shows the interscale enstrophy transfer ( $\langle P_z \rangle = \langle \Pi \omega \rangle$ ) of RL-Leith, DSmag, and DLeith compared with the reference  $\langle P_z \rangle$  obtained from filtering the DNS results. The RL-Leith model outperforms DSmag and DLeith in predicting the true enstrophy interscale transfer. This is likely due to the ability of RL-Leith to capture backscattering (transfer from subgrid to resolved scales), resulting in less diffusion than DSmag and DLeith. We also observe that DLeith outperforms DSmag in all 4 cases, demonstrating the benefits of using the Leith form of the eddy-viscosity model rather than the Smagorinsky form in LES of 2D turbulence, where capturing enstrophy interscale transfer is essential. The advantage of DLeith over DSmag in terms of capturing the interscale enstrophy transfer is also reflected on *a-posteriori* analysis, see Fig. 2.

#### 3.3 Interpretability of the SMARL model

To understand the superior performance of RL-Leith over the classical SGS models, we compare the distribution of Leith coefficients  $c_l$  obtained from RL-Leith and DLeith. The first column of Fig. 4 shows the PDF of the Leith model coefficients  $c_l$  for the four cases. In all cases, the coefficients obtained with the DLeith model are concentrated around some positive values (rare negative values have been removed with positive clipping, which is essential for the LES stability with DLeith and DSmag [22, 20]). This leads to excessive diffusion, also confirmed by Figs. 2 and 3. In contrast, the Leith coefficients learned from RL-Leith spread across a much wider range of values than DLeith, and include negative values (LES with Leith-RL remains stable despite these negative viscosities). This shows that the RL-Leith model captures both the forward/diffusive and backscatter inter-scale energy/enstrophy transfer. Similarly to DLeith, the majority of the coefficients predicted by RL-Leith is positive, showing that the RL-Leith model is more likely to be diffusive in general. However, the highest probability density of the coefficients obtained with RL-Leith occurs closer to 0, especially for Cases 3 and 4, indicating that the RL-Leith is less diffusive than DLeith.

The second and third columns of Fig. 4 show the sensitivity of the model to its inputs. This is shown through the first-order and total Sobol indices of the model policy (see Section B for details). It decomposes

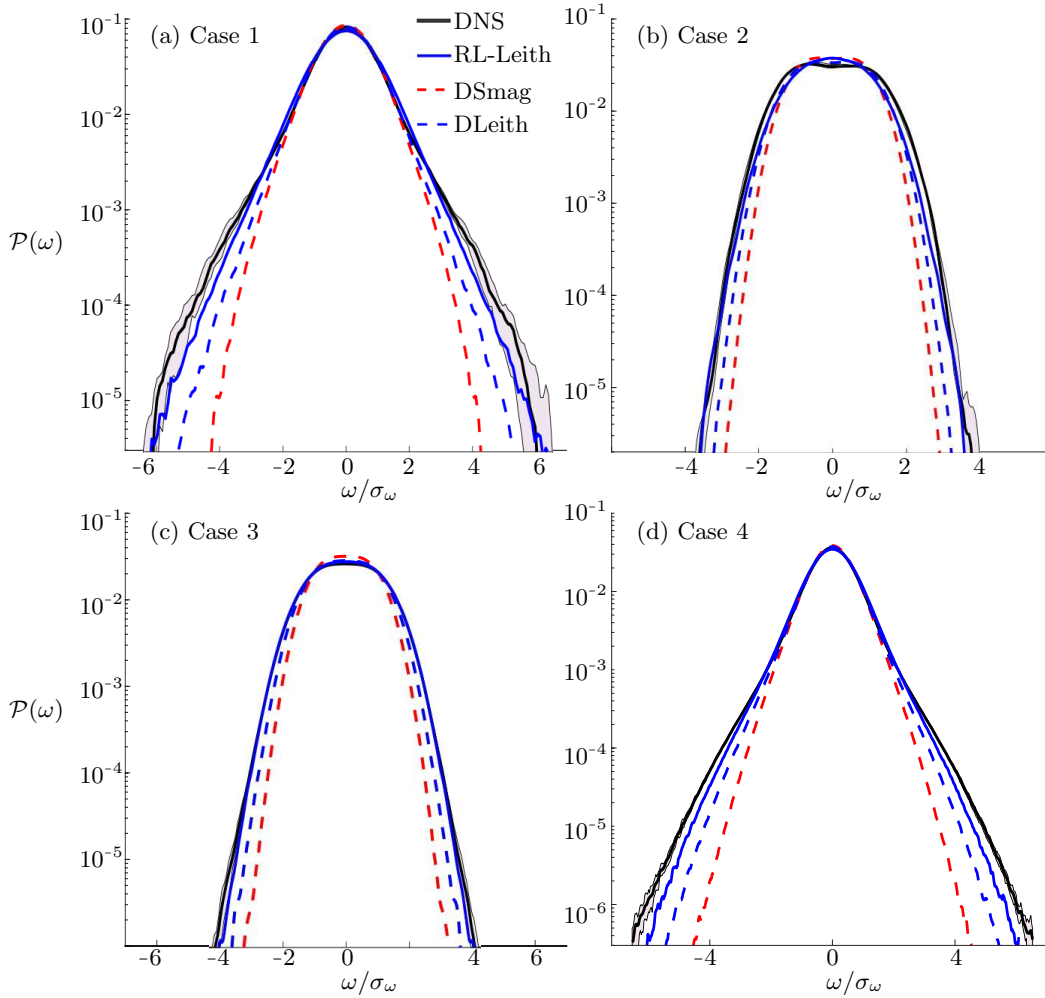


Figure 2: *A-posteriori* testing results in terms of the PDF of vorticity ( $\mathcal{P}(\omega)$ ). The  $x$ -axis is normalized by the standard deviation of vorticity ( $\sigma_\omega$ ) computed from DNS of each case. The shading area represents the uncertainty (25-75 quartiles) of the DNS PDF.

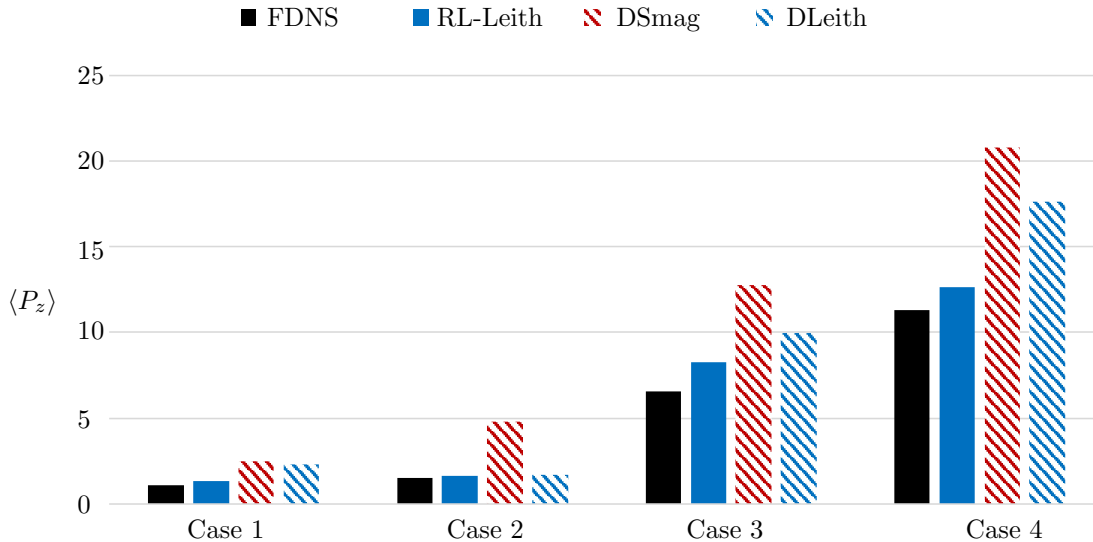


Figure 3: Total enstrophy diffusion  $\langle P_z \rangle$  obtained from the FDNS, RL-Leith, DSmag and DLeith for the four cases.

the variance of the model output into contributions from: (1) each individual input (first-order Sobol index  $S_k$ ), and (2) interaction among inputs (total Sobol index  $S_{T,k}$ ). In all cases, the model output is more sensitive to the low-wavenumber entries of the enstrophy spectrum. This observation is consistent with the fact that most of the kinetic energy and enstrophy is contained in the large scales, corresponding to low wavenumbers  $k$ . For example, the ratio of turbulent kinetic energy  $\langle \hat{E}(k < k_f) \rangle_k / \langle \hat{E}(k) \rangle_k = 92.6\%$  for Case 1, 94.5% for Case 2, 92.3% for Case 3, and 93.4% for Case 4. In 2D turbulence, this region also coincides with the inverse energy cascade region,  $k < k_f$ , where  $k_f$  is the forcing wavenumber of the 2D turbulence systems at which energy is injected into the flow (see Section 5). The next significant region is near the Nyquist wavenumber  $k_c$ , i.e. the maximum wavenumber in the LES simulations. This region is responsible for interscale energy and enstrophy transfer between the resolved and unresolved scales. Therefore, changes of  $\hat{Z}$  at this wavenumber immediately trigger a change in the closure coefficient  $c_l$ . The Sobol indices suggest that the enstrophy contained in the middle wavenumber range does not have a significant impact on the leard coefficients  $c_l$ , and thus the learned viscosity.

### 3.4 Generalization to higher Reynolds numbers

The generalization capability of data-driven SGS models across different flow regimes (e.g., higher  $Re$  turbulent flows) is essential for their practical use. However, many deep-learning-based SGS models do not generalize well and often require extra data or training efforts, such as transfer learning [20, 25] to be successful. Training data for high- $Re$  turbulent flows are especially difficult to obtain. For example, Case 5 has  $15\times$  higher  $Re$  than Case 1, and therefore DNS to resolve Case 5 requires  $16\times$  higher spatial resolution compared to Case 1 and correspondingly higher temporal resolution due to Courant-Friedrichs-Lewy condition. In Fig. 5 we show that the RL-Leith closure trained on Case 1 can be directly used for Case 5 without any new data from Case 5 or an additional training process. It can be observed that the RL-Leith trained on Case 1 is fully generalizable to work on LES of Case 5. Similar to the testing for Case 1, the RL-Leith model outperforms DSmag in terms of matching the DNS kinetic energy spectra,  $\hat{E}(k)$ , and it outperforms both physics-based models (DSmag and DLeith) in matching the DNS  $\mathcal{P}(\omega)$  for Case 5 down to the tails (extreme events). The generalization capability of SMARL-based SGS models to higher  $Re$  turbulence can be explained by the state-action map that is trained during the RL online learning. As the state,  $s'(t)$ , is the enstrophy spectrum,  $\hat{Z}(k, t)$ , the difference between  $Re = 20,000$  (Case 1) and  $Re = 300,000$  (Case 5)

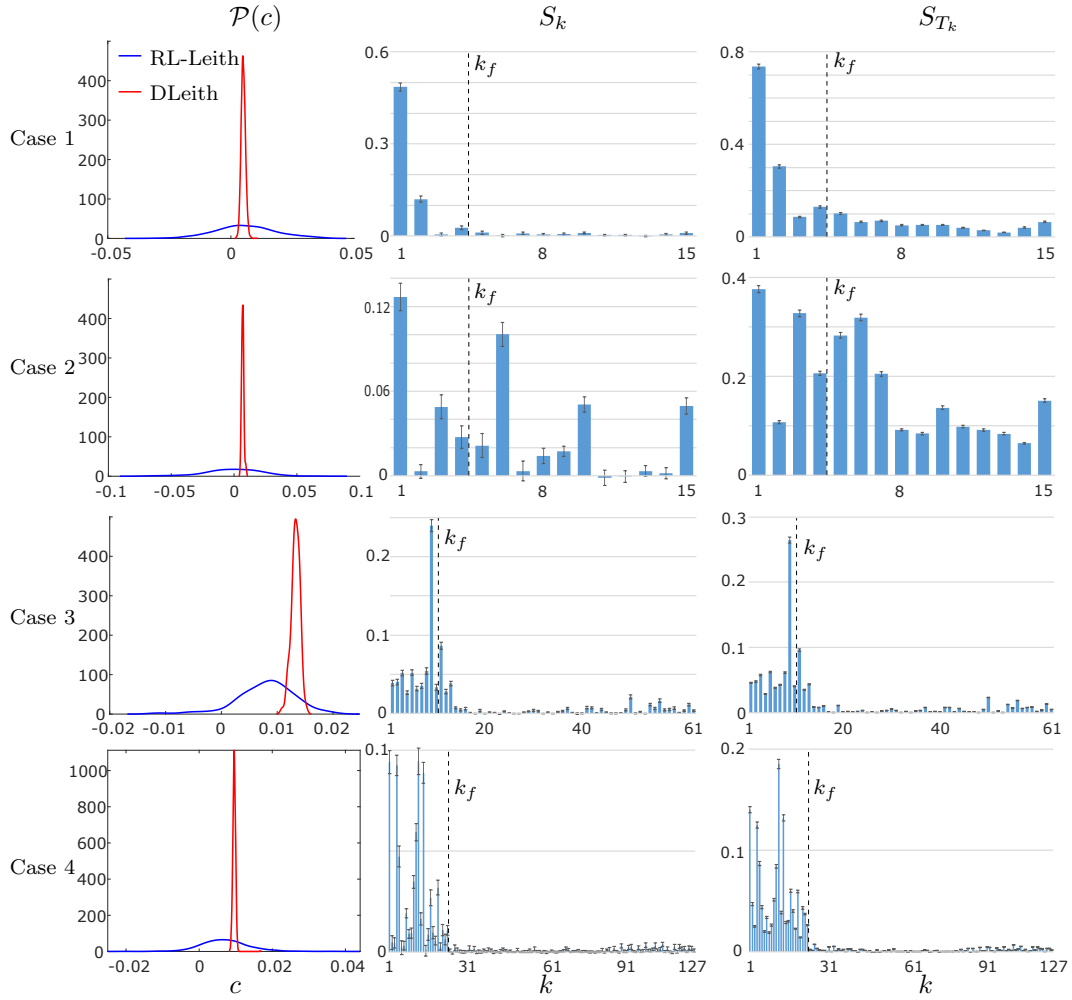


Figure 4: First column: PDF of model coefficients  $c$ ; second column:  $S_k$ ; and third column:  $S_{T_k}$ . The error bars on the Sobol indices indicate 95% confidence level. The Nyquist (or cut-off) wavenumber  $k_c$  is the maximum wavenumber (i.e.,  $k_c = 15$  in Case 1 and 2,  $k_c = 61$  in Case 3, and  $k_c = 127$  in Case 4). The dash lines in second and third columns mark the forcing wavenumber  $k_f$ .

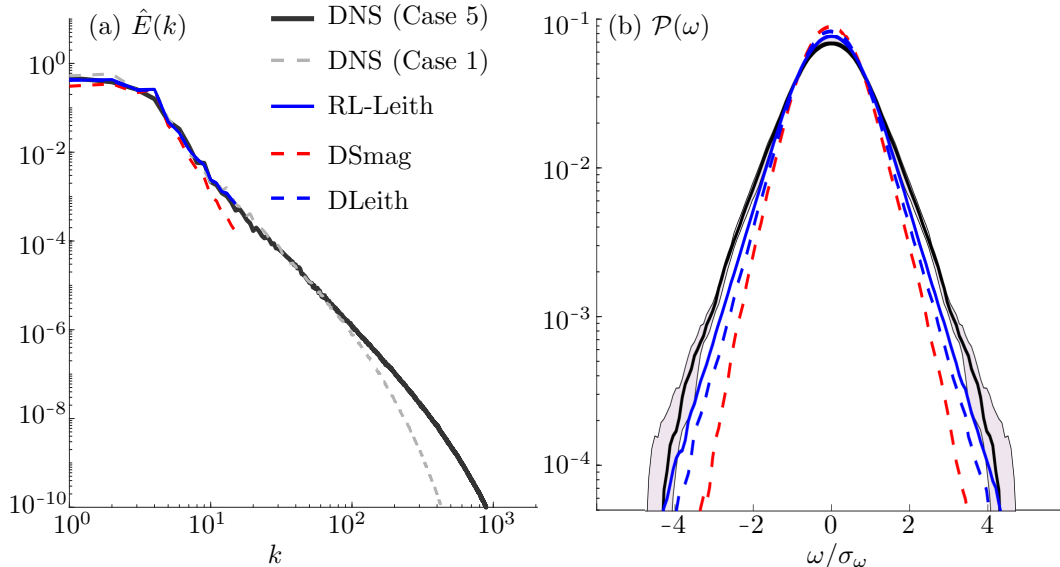


Figure 5: Generalization testing of SMARL to higher ( $15 \times Re$ ) turbulence (SMARL trained on Case 1 and tested on Case 5). (a) shows the turbulent kinetic energy spectra,  $\hat{E}(k)$ , and (b) shows the PDF,  $\mathcal{P}(\omega)$ . In (b), the  $x$ -axis is normalized by the standard deviation of vorticity ( $\sigma_\omega$ ) computed from DNS. The shading area represents the uncertainty (25-75 quartiles) of the DNS PDF.

lies only in the smallest scales that can only be resolved in DNS. When the LES uses an aggressive (small) cut-off wavenumber (e.g., here for both Case 1 and 5,  $k_c = 16$ ), the cut-off  $\hat{Z}_{\text{DNS}}(k, t)$  is very similar between Case 1 and 5, see Fig. 5 for the comparison between the energy spectrum,  $\hat{E}(k)$ , of Case 1 and 5.

## 4 Conclusions

We have introduced a data-efficient, SMARL-based framework to learn LES closures for geophysical turbulence with broad potential applications to climate modeling. This framework is superior to existing AI-based closure modeling approaches as it works with: (i) sparse amounts of training data that are insufficient for supervised learning based on DNN [61] and (ii) low LES resolutions inaccessible to closures identified with equation discovery [21]. Furthermore, the framework does not need a differentiable numerical solver and implicitly addresses model structural errors [40, 62].

We show that these closures enable LES to produce statistics, including energy spectra, PDF, and most importantly, tails of the PDFs, that closely match those of the far more expensive DNS. Moreover, LES with SMARL-based closures significantly outperform LES with classical physics-based closures in capturing extreme events, which are often diffusive to ensure stability but then underestimate extremes. With a small number of samples from DNS, SMARL develops closures capable of capturing the statistics of such extreme events, suggesting that both diffusion and backscattering, i.e., the two-way interaction of the resolved scales and SGS, are accurately represented. We emphasize that the LES cases investigated here have 160 to  $163,840 \times$  spatio-temporally coarser resolution compared to their DNS. LES+SMARL is stable and can easily run thoughts of times longer than the lengths of the training set and training horizon.

We provide an interpretation of the SMARL-based closure by analysing the state-action map learned using SMARL with the Sobol indices. Their distribution across wavenumber,  $k$  in the enstrophy spectrum indicate that large-scale structures that contain most of the kinetic energy and enstrophy, have the most contribution to the prediction of the closure’s coefficient  $c_l$ . The next significant contribution stems from the high-wavenumber region near the cut-off wavenumber,  $k_c$ . This can be interpreted as the directly responsible region of interscale energy and enstrophy transfer.

We have tested the generalization of the SMARL-based closure by testing a pre-trained DNN to a different

flow regime where the  $Re$  is increased by  $15\times$ . LES test shows that the SMARL-based closure, albeit trained at a lower  $Re$ -number flow, performs better than DLeith and DSmag in terms of matching the kinetic energy spectrum and the PDF of vorticity,  $\mathcal{P}(\omega)$ , even at the tails of the distribution, corresponding to extreme vorticity events.

In summary, we demonstrate a SMARL-based framework to develop novel, accurate, stable, and generalizable SGS closure for geophysical turbulence, which can be scaled up to GCMs and Earth system models in the future.

## Acknowledgments

We thank Pascal Weber (Manukai) for the discussions on Korali. PK and PH gratefully acknowledge support from the Salata Institute Climate project (GSD)-032549 and NSF CSSI Program (OAC-2005123), respectively.

## 5 Methods

### 5.1 Direct and large-eddy simulations of 2D turbulence

We consider two-dimensional flows expressed in the vorticity ( $\omega$ ) and stream function ( $\psi$ ) formulation in a doubly periodic square domain with length  $L = 2\pi$ ,

$$\frac{\partial \omega}{\partial t} + \mathcal{N}(\omega, \psi) = \frac{1}{\text{Re}} \nabla^2 \omega - f - r\omega + \beta \frac{\partial \psi}{\partial x}, \quad (2a)$$

$$\nabla^2 \psi = -\omega, \quad (2b)$$

where  $\mathcal{N}(\omega, \psi) = (\partial \psi / \partial y) (\partial \omega / \partial x) - (\partial \psi / \partial x) (\partial \omega / \partial y)$ , is the nonlinear advection term, and  $f(x, y) = \kappa_f [\cos(\kappa_f x) + \cos(\kappa_f y)]$  is a deterministic forcing [63, 64]. To obtain target statistics, we solve Eq. (2) numerically. A Fourier-Fourier pseudo-spectral solver is used to solve these equations, see e.g. [21, 20, 25]. The computational grid has uniform spacing  $\Delta_{\text{DNS}} = L/N_{\text{DNS}}$ , where  $N_{\text{DNS}}$  is the number of grid points in each direction, as shown in Table 1. The time-stepping size is  $\Delta t_{\text{DNS}} = 5 \times 10^{-5}$  dimensionless time unit for cases 1, 2, 3, 4 and  $\Delta t_{\text{DNS}} = 1 \times 10^{-5}$  dimensionless time unit for cases 5. Once the flow reaches statistical equilibrium after a long-term spin-up, we uniformly sample 5 snapshots that are  $10000 \Delta t_{\text{DNS}}$  apart to obtain decorrelated data to generate the reference enstrophy spectra, following [59, 40].

We perform filtered direct numerical simulation (FDNS) by applying a sharp Fourier cut-off filter (cut-off wavenumber  $k_c = \pi/\Delta_{\text{FDNS}}$ ) to each variable in Eq. (2), denoted by  $\bar{\cdot}$ , along each of  $x$  and  $y$  directions [55, 49]:

$$\frac{\partial \bar{\omega}}{\partial t} + \mathcal{N}(\bar{\omega}, \bar{\psi}) = \frac{1}{\text{Re}} \nabla^2 \bar{\omega} - \bar{f} - r\bar{\omega} + \beta \frac{\partial \bar{\psi}}{\partial x} + \underbrace{\mathcal{N}(\bar{\omega}, \bar{\psi}) - \overline{\mathcal{N}(\omega, \psi)}}_{\Pi = \nabla \times (\nabla \cdot \tau^{\text{SGS}})}, \quad (3a)$$

$$\nabla^2 \bar{\psi} = -\bar{\omega}. \quad (3b)$$

The LES equation is the same as Eq. (3) except for the unclosed SGS term  $\Pi$ . The LES is solved on a coarse resolution  $\Delta_{\text{LES}} = \Delta_{\text{FDNS}}$  with  $\Pi$  modeled as a map connecting the resolved flow variables to the closure term. The LES is solved with the same numerical method as the DNS, with grid spacing  $\Delta_{\text{LES}} = L/N_{\text{LES}}$  and time step  $\Delta t_{\text{LES}} = 10 \Delta t_{\text{DNS}}$ .

### 5.2 SMARL setup

$N$  agents are distributed uniformly on the grid of the simulation domain. Agents can sense states  $s^{(i)}(t)$  and perform actions according to a shared policy,  $a^{(i)}(t) \sim \pi(\cdot | s^{(i)}(t))$ . In this work, we use global states only, meaning that  $s^{(i)}(t) = s'(t)$  for any agent  $i$ . In the appendix, we show that adding local states to the input of the policy does not improve the results. The choice of using the same policy,  $\pi(\cdot | s^{(i)}(t))$ , for every agent is motivated by the translation invariance of the Navier-Stokes equations. The selection of states, actions, and rewards is critical to the performance of SMARL as detailed below.

**States.** Each agent observes the enstrophy spectrum of the LES,  $s'(t) = \hat{Z}_{\text{LES}}(k, t)$ . We found that adding the five Galilean-invariant quantities derived from filtered velocity gradients and Hessians [65, 41] did not improve the performance of the closure model (Section B).

**Action.** The agents control local coefficients  $c_l(x, y, t)$  in traditional eddy-viscosity closures: Leith model [48]. These coefficients are evaluated at the agents' locations and then interpolated onto the LES grid. The interpolated coefficients are then used to compute the subgrid stress tensor  $\tau^{\text{SGS}} = -2\nu_e \bar{\mathcal{S}}$ , which enters the LES solver. Actions are evaluated every 10 time steps of the LES solver, and local coefficients are kept constant between two consecutive actions.

**Reward.** The objective of the agents is to learn a closure that matches the DNS enstrophy spectrum. Thus, we have chosen the instantaneous reward to be large when the enstrophy spectrum is close to the reference,

$$r(t) = \frac{1}{\|\log \hat{Z}_{\text{DNS}}(k) - \log \hat{Z}_{\text{LES}}(k, t)\|_2^2}, \quad (4)$$

where  $\hat{Z}_{\text{DNS}}$  is the spectrum obtained from DNS simulations. This reference spectrum is computed from short DNS trajectories, which are known to be insufficient for purely offline training [59]. Furthermore, these DNS trajectories are much shorter than what would be required to capture the rare events that we report in the results section.

### 5.3 Training algorithm: V-RACER

The training of the policy is performed with the V-RACER algorithm with Remember and Forget experience replay (ReFER) [66], adapted to multi-agent settings as described in Weber et. al. [67] and implemented in the software Korali [68]. Here, we describe the main components of the training algorithm.

At each time step  $t$ , agents observe the state  $s'(t)$ , perform an action sampled from the behavior policy  $a(t) \sim \mu_t(\cdot, s'(t))$ , and transition to a new state  $s'(t + \Delta t)$  following the dynamics of the model (e.g., LES solver with SMARL-based closure here), with reward  $r(t + \Delta t)$ . Experiences  $\{s'(t), a(t), s'(t + \Delta t), r(t), \mu_t\}$  are stored in a replay buffer. In V-RACER, the policy  $\pi^\theta(\cdot, s)$  is represented as a Gaussian with mean  $m^\theta(s)$  and covariance  $\Sigma^\theta(s)$ , which, in addition to the value  $V^\theta(s)$ , are the output of a single neural network with weights  $\theta$  and input  $s$ .

The weights  $\theta$  are updated to minimize two losses, corresponding to the off-policy objective and to match the value function with an on-policy value estimate. We use the Adam gradient-based optimization method to minimize these objectives. The off-policy objective is used to update the policy weights:

$$\mathcal{L}^{\text{off-PG}}(\theta) = -\mathbb{E}_{s_k \sim B, a_k \sim \mu_k(s_k)} \left[ \rho_k \left( \hat{Q}_t^{\text{ret}} - V^\theta(s_k) \right) \right], \quad (5)$$

where  $B(s) \propto \sum_{k=t-N}^t P(s_k = s | s_0, a_k \sim \mu_k)$  is the probability of sampling the state  $s$  from the replay memory containing the past  $N$  experiences of the agent acting with policy  $\mu_k$ . Furthermore, the importance weight is defined as  $\rho_k = \pi^\theta(s_k | a_k) / \mu_k(s_k | a_k)$ , and the on-policy returns are estimated as

$$\hat{Q}_{t-1}^{\text{ret}} = r_t + \gamma V^\theta(s_t) | \gamma \bar{\rho}_t \left[ \hat{Q}_t^{\text{ret}} - V^\theta(s_t) \right], \quad (6)$$

with  $\bar{\rho}_t = \min\{1, \rho_t\}$ . The on-policy state-value is estimated from  $V^\theta$  using the recursive formula [66]

$$\hat{V}_t^{\text{tbc}} = V^\theta(s_t) + \bar{\rho}_t \left[ r_{t+1} + \gamma \hat{V}_{t+1}^{\text{tbc}} - V^\theta(s_t) \right]. \quad (7)$$

This estimate is part of the loss used to train the value function:

$$\mathcal{L}^{\text{tbc}}(\theta) = \frac{1}{2} \mathbb{E}_{s_k \sim B, a_k \sim \mu_k(s_k)} \left[ V^\theta(s_t) - \hat{V}_t^{\text{tbc}} \right]^2. \quad (8)$$

The gradients of these losses are updated according to the ReF-ER procedure [66]. This consists of clipping gradients to zero when the importance weight is outside of the interval  $[1/c_{\text{max}}, c_{\text{max}}]$ , where  $c_{\text{max}}$  is a positive constant. Furthermore, the gradients are biased towards the direction of past behaviors,

$$\mathbf{g}_t^{\text{ReF-ER}}(\theta) = \beta \mathbf{g}_t(\theta) - (1 - \beta) \nabla D_{\text{KL}} \left[ \mu_t(\cdot | s_t) || \pi^\theta(\cdot | s_t) \right], \quad (9)$$

where  $\beta > 0$  is a hyper-parameter and  $D_{\text{KL}}$  represents the KL-divergence between two distributions.

## 5.4 State-action map sensitivity analysis

To determine the effects of the SMARL DNN input ( $\hat{Z}(k, t)$ ) at each wavenumber  $k$  to the NN output ( $c_l(t) = f_{\text{DNN}}(\hat{Z}(k, t))$ ), we use the Sobol index which decomposes the variance of the output into contributions from: (1) each individual input, and (2) interaction among inputs. The variance of  $c_l$  can be decomposed as:

$$\text{Var}(c_l) = \sum_m \xi_m + \sum_{m < n} \xi_{mn} + \dots + \xi_{1,2,3,\dots,k_c}, \quad (10)$$

where here  $\xi_m = \text{Var}(\mathbb{E}(c_l | \hat{Z}(m)))$  are the partial variances associated with one component of the decomposition. The first-order Sobol index is defined as

$$S_j = \frac{\xi_j}{\text{Var}(c_l)}, \quad (11)$$

which is the fraction of output variance explained by varying  $\hat{Z}(k = k_j)$  alone. The total index:

$$S_{T_j} = 1 - \frac{\xi_{\sim j}}{\text{Var}(c_l)}, \quad (12)$$

which is the fraction of output variance explained by varying  $\hat{Z}(k_j)$  and all interactions involving it.  $\xi_{\sim j}$  is the variance of  $c_l$  while holding  $\hat{Z}(k_j)$  fixed.

## 5.5 Experiments and test cases

We have developed closures for 5 different forced 2D turbulent flows (2 with the  $\beta$ -plane effects; details in Table 1). These cases are commonly used to evaluate the SGS closures of geophysical turbulence [69, 59, 24] and exhibit distinct behaviors and dynamics, as seen in snapshots of vorticity fields,  $\omega$ , in Fig. 1. Training is performed with the objective of achieving an LES enstrophy spectrum close to the target DNS spectrum. We also compare the kinetic energy spectra in Section A. Additionally, to test the predictability of SMARL-based LES models for extreme events, we compare the PDFs of the resolved vorticity,  $\mathcal{P}(\omega)$ . The tails of these PDFs represent rare, extreme events, i.e., significantly large  $\omega$  with a small probability of occurrence. Note that these vortices resemble the weather system’s high- and low-pressure anomalies, which can cause various extreme weather events [70]. LES with 16 to 16,384 $\times$  coarser spatial resolution and 10 $\times$  larger time steps coupled to the learned closures are then tested with the SMARL-based closures, and their statistics are compared with those of the DNS and LES with classical dynamic Smagorinsky and Leith closures. As summarized in Fig. 2, the tails of the vorticity PDFs clearly show the advantage of the SMARL-based closures, suggesting that these closures have the right amount of diffusion and backscattering (anti-diffusion). The classical closures are too diffusive and underestimate extreme events. The energy spectra also show the better ability of LES with SMARL-based closures in capturing the energy across the scales.

Table 1: The test cases and hyper-parameters in training.  $\sigma_\omega$  is standard deviation of vorticity.

Case	Re	$\beta$	$\kappa_f$	$\sigma_\omega$	$N_{\text{DNS}}$	$N_{\text{LES}}$	$\Delta t_{\text{RL}}/\Delta t_{\text{LES}}$	Training horizon	Testing horizon
1	$20 \times 10^3$	0	4	5.51	1024	32	10	$10^3 \Delta t_{\text{RL}}$	$10^6 \Delta t_{\text{RL}}$
2	$20 \times 10^3$	20	4	10.75	1024	32	10	$10^3 \Delta t_{\text{RL}}$	$10^6 \Delta t_{\text{RL}}$
3	$20 \times 10^3$	50	10	13.14	1024	128	10	$10^3 \Delta t_{\text{RL}}$	$10^6 \Delta t_{\text{RL}}$
4	$20 \times 10^3$	0	25	13.47	1024	256	10	$10^3 \Delta t_{\text{RL}}$	$10^6 \Delta t_{\text{RL}}$
5	$300 \times 10^3$	0	4	6.42	4096	32	10	$10^3 \Delta t_{\text{RL}}$	$10^6 \Delta t_{\text{RL}}$

## References

- [1] Richard S.J. Tol. A meta-analysis of the total economic impact of climate change. *Energy Policy*, 185:113922, 2024.
- [2] Jonathan Anchen, Victor Blanco Gonzalez, Mitali Chatterjee, Rainer Egloff, Andreas Felderer, Anna Mejlerö, Anja Vischer, and Bernd Wilke. Swiss Re SONAR: New emerging risk insights. Technical report, Swiss Re Institute, Zurich, Switzerland, June 2025.
- [3] Kristie L Ebi, Jennifer Vanos, Jane W Baldwin, Jesse E Bell, David M Hondula, Nicole A Errett, Katie Hayes, Colleen E Reid, Shubhayu Saha, June Spector, et al. Extreme weather and climate change: population health and health system implications. *Annual review of public health*, 42(1):293–315, 2021.
- [4] IPCC. *Climate Change 2021: The Physical Science Basis. Contribution of Working Group I to the Sixth Assessment Report of the Intergovernmental Panel on Climate Change*. Cambridge University Press, 2021.
- [5] IPCC. *Climate Change 2022: Impacts, Adaptation and Vulnerability. Contribution of Working Group II to the Sixth Assessment Report of the Intergovernmental Panel on Climate Change*. Cambridge University Press, 2022.
- [6] David Randall, Marat Khairoutdinov, Akio Arakawa, and Wojciech Grabowski. Breaking the cloud parameterization deadlock. *Bulletin of the American Meteorological Society*, 84(11):1547–1564, 2003.
- [7] Helene T Hewitt, Malcolm Roberts, Pierre Mathiot, Arne Biastoch, Ed Blockley, Eric P Chassignet, Baylor Fox-Kemper, Pat Hyder, David P Marshall, Ekaterina Popova, et al. Resolving and parameterising the ocean mesoscale in earth system models. *Current Climate Change Reports*, pages 1–16, 2020.
- [8] Baylor Fox-Kemper, Alistair Adcroft, Claus W Böning, Eric P Chassignet, Enrique Curchitser, Gokhan Danabasoglu, Carsten Eden, Matthew H England, Rüdiger Gerdes, Richard J Greatbatch, et al. Challenges and prospects in ocean circulation models. *Frontiers in Marine Science*, 6:65, 2019.
- [9] Tim Palmer. Climate forecasting: Build high-resolution global climate models. *Nature*, 515(7527):338–339, 2014.
- [10] Julia Slingo and Tim Palmer. Uncertainty in weather and climate prediction. *Philosophical Transactions of the Royal Society A: Mathematical, Physical and Engineering Sciences*, 369(1956):4751–4767, 2011.
- [11] Ching-Yao Lai, Pedram Hassanzadeh, Aditi Sheshadri, Maike Sonnewald, Raffaele Ferrari, and Venkaramani Balaji. Machine learning for climate physics and simulations. *Annual Review of Condensed Matter Physics*, 16(1):343–365, 2025.
- [12] Annalisa Bracco, Julien Brajard, Henk A Dijkstra, Pedram Hassanzadeh, Christian Lessig, and Claire Monteleoni. Machine learning for the physics of climate. *Nature Reviews Physics*, 7(1):6–20, 2025.
- [13] Oliver Watt-Meyer, Brian Henn, Jeremy McGibbon, Spencer K. Clark, Anna Kwa, W. Andre Perkins, Elynn Wu, Lucas Harris, and Christopher S. Bretherton. ACE2: Accurately learning subseasonal to decadal atmospheric variability and forced responses. *npj Climate and Atmospheric Science*, 8(205 (2025)), 2025.
- [14] Shahine Bouabid, Andre Nogueira Souza, and Raffaele Ferrari. Score-based generative emulation of impact-relevant earth system model outputs. *arXiv preprint arXiv:2510.04358*, 2025.
- [15] Tianyi Li, Luca Biferale, Fabio Bonaccorso, Martino Andrea Scarpolini, and Michele Bucciotti. Synthetic lagrangian turbulence by generative diffusion models. *Nature Machine Intelligence*, 6(4):393–403, 2024.

- [16] Amaury Lancelin, Alex Wikner, Laurent Dubus, Clément Le Priol, Dorian S Abbot, Freddy Bouchet, Pedram Hassanzadeh, and Jonathan Weare. AI-boosted rare event sampling to characterize extreme weather. *arXiv preprint arXiv:2510.27066*, 2025.
- [17] Y. Qiang Sun, Pedram Hassanzadeh, Mohsen Zand, Ashesh Chattopadhyay, Jonathan Weare, and Dorian S. Abbot. Can AI weather models predict out-of-distribution gray swan tropical cyclones? *Proceedings of the National Academy of Sciences*, 122(21):e2420914122, May 2025.
- [18] Tapio Schneider, Swadhin Behera, Giulio Boccaletti, Clara Deser, Kerry Emanuel, Raffaele Ferrari, L Ruby Leung, Ning Lin, Thomas Müller, Antonio Navarra, et al. Harnessing AI and computing to advance climate modelling and prediction. *Nature Climate Change*, 13(9):887–889, 2023.
- [19] Ian Grooms, Nora Loose, Ryan Abernathy, JM Steinberg, Scott Daniel Bachman, Gustavo Marques, Arthur Paul Guillaumin, and Elizabeth Yankovsky. Diffusion-based smoothers for spatial filtering of gridded geophysical data. *Journal of Advances in Modeling Earth Systems*, 13(9):e2021MS002552, 2021.
- [20] Yifei Guan, Ashesh Chattopadhyay, Adam Subel, and Pedram Hassanzadeh. Stable a posteriori LES of 2D turbulence using convolutional neural networks: Backscattering analysis and generalization to higher Re via transfer learning. *Journal of Computational Physics*, 458:111090, 2022.
- [21] Karan Jakhar, Yifei Guan, Rambod Mojjani, Ashesh Chattopadhyay, and Pedram Hassanzadeh. Learning closed-form equations for subgrid-scale closures from high-fidelity data: Promises and challenges. *Journal of Advances in Modeling Earth Systems*, 16(7):e2023MS003874, 2024.
- [22] Romit Maulik, Omer San, Adil Rasheed, and Prakash Vedula. Subgrid modelling for two-dimensional turbulence using neural networks. *Journal of Fluid Mechanics*, 858:122–144, 2019.
- [23] Thomas Bolton and Laure Zanna. Applications of deep learning to ocean data inference and subgrid parameterization. *Journal of Advances in Modeling Earth Systems*, 11(1):376–399, 2019.
- [24] Kaushik Srinivasan, Mickael D Chekroun, and James C McWilliams. Turbulence closure with small, local neural networks: Forced two-dimensional and  $\beta$ -plane flows. *Journal of Advances in Modeling Earth Systems*, 16(4):e2023MS003795, 2024.
- [25] Adam Subel, Yifei Guan, Ashesh Chattopadhyay, and Pedram Hassanzadeh. Explaining the physics of transfer learning in data-driven turbulence modeling. *PNAS nexus*, 2(3):pgad015, 2023.
- [26] Malte F. Jansen, Isaac M. Held, Alistair Adcroft, and Robert Hallberg. Energy budget-based backscatter in an eddy permitting primitive equation model. *Ocean Modelling*, 94:15–26, 2015.
- [27] Paul A O’Gorman and John G Dwyer. Using machine learning to parameterize moist convection: Potential for modeling of climate, climate change, and extreme events. *Journal of Advances in Modeling Earth Systems*, 10(10):2548–2563, 2018.
- [28] Y Qiang Sun, Pedram Hassanzadeh, M Joan Alexander, and Christopher G Kruse. Quantifying 3d gravity wave drag in a library of tropical convection-permitting simulations for data-driven parameterizations. *Journal of Advances in Modeling Earth Systems*, 15(5):e2022MS003585, 2023.
- [29] Karan Jakhar, Yifei Guan, and Pedram Hassanzadeh. Analytical and ai-discovered stable, accurate, and generalizable subgrid-scale closure for geophysical turbulence. *Phys. Rev. Lett.*, 136:064201, Feb 2026.
- [30] Hamid A Pahlavan, Pedram Hassanzadeh, and M Joan Alexander. Explainable offline-online training of neural networks for parameterizations: A 1d gravity wave-qbo testbed in the small-data regime. *Geophysical Research Letters*, 51(2):e2023GL106324, 2024.

- [31] Tapio Schneider, Andrew M Stuart, and Jin-Long Wu. Learning stochastic closures using ensemble Kalman inversion. *Transactions of Mathematics and Its Applications*, 5(1):tnab003, 2021.
- [32] Tapio Schneider, Shiwei Lan, Andrew Stuart, and Joao Teixeira. Earth system modeling 2.0: A blueprint for models that learn from observations and targeted high-resolution simulations. *Geophysical Research Letters*, 44(24):12–396, 2017.
- [33] Hugo Frezat, Julien Le Sommer, Ronan Fablet, Guillaume Balarac, and Redouane Lguensat. A posteriori learning for quasi-geostrophic turbulence parametrization. *Journal of Advances in Modeling Earth Systems*, 14(11):e2022MS003124, 2022.
- [34] Varun Shankar, Dibyajyoti Chakraborty, Venkatasubramanian Viswanathan, and Romit Maulik. Differentiable turbulence: Closure as a partial differential equation constrained optimization. *Physical Review Fluids*, 10(2):024605, 2025.
- [35] M. Gelbrecht, A. White, S. Bathiany, and N. Boers. Differentiable programming for earth system modeling. *EGU sphere*, 2022:1–17, 2022.
- [36] Nikola B Kovachki and Andrew M Stuart. Ensemble kalman inversion: a derivative-free technique for machine learning tasks. *Inverse Problems*, 35(9):095005, 2019.
- [37] Oliver RA Dunbar, Alfredo Garbuno-Inigo, Tapio Schneider, and Andrew M Stuart. Calibration and uncertainty quantification of convective parameters in an idealized GCM. *Journal of Advances in Modeling Earth Systems*, 13(9):e2020MS002454, 2021.
- [38] Tapio Schneider, Andrew M Stuart, and Jin-Long Wu. Imposing sparsity within ensemble Kalman inversion. *arXiv preprint arXiv:2007.06175*, 2020.
- [39] Vincent Mons, Yifan Du, and Tamer A Zaki. Ensemble-variational assimilation of statistical data in large-eddy simulation. *Physical Review Fluids*, 6(10):104607, 2021.
- [40] Yifei Guan, Pedram Hassanzadeh, Tapio Schneider, Oliver Dunbar, Daniel Zhengyu Huang, Jinlong Wu, and Ignacio Lopez-Gomez. Online learning of eddy-viscosity and backscattering closures for geophysical turbulence using ensemble kalman inversion. *arXiv preprint arXiv:2409.04985*, 2024.
- [41] Guido Novati, Hugues Lascombes de Laroussilhe, and Petros Koumoutsakos. Automating turbulence modelling by multi-agent reinforcement learning. *Nature Machine Intelligence*, 3(1):87–96, 2021.
- [42] Marius Kurz, Philipp Offenhäuser, and Andrea Beck. Deep reinforcement learning for turbulence modeling in large eddy simulations. *International Journal of Heat and Fluid Flow*, 99:109094, 2023.
- [43] H Jane Bae and Petros Koumoutsakos. Scientific multi-agent reinforcement learning for wall-models of turbulent flows. *Nature Communications*, 13(1):1443, 2022.
- [44] Junhyuk Kim, Hyojin Kim, Jiyeon Kim, and Changhoon Lee. Deep reinforcement learning for large-eddy simulation modeling in wall-bounded turbulence. *Physics of Fluids*, 34(10), 2022.
- [45] Dmitrii Kochkov, Janni Yuval, Ian Langmore, Peter Norgaard, Jamie Smith, Griffin Mooers, Milan Klöwer, James Lottes, Stephan Rasp, Peter Düben, Sam Hatfield, Peter Battaglia, Alvaro Sanchez-Gonzalez, Matthew Willson, Michael P. Brenner, and Stephan Hoyer. Neural general circulation models for weather and climate, 2024.
- [46] Karan Jakhar, Yifei Guan, and Pedram Hassanzadeh. Analytical and AI-discovered stable, accurate, and generalizable subgrid-scale closure for geophysical turbulence. *Phys. Rev. Lett.*, 136:064201, Feb 2026.
- [47] Joseph Smagorinsky. General circulation experiments with the primitive equations: I. the basic experiment. *Monthly Weather Review*, 91(3):99 – 164, 1963.

- [48] Cecil E. Leith. Stochastic models of chaotic systems. *Physica D: Nonlinear Phenomena*, 98(2):481–491, 1996. Nonlinear Phenomena in Ocean Dynamics.
- [49] Pierre Sagaut. *Large eddy simulation for incompressible flows: An introduction*. Springer Science & Business Media, 2006.
- [50] Massimo Germano, Ugo Piomelli, Parviz Moin, and William H Cabot. A dynamic subgrid-scale eddy viscosity model. *Physics of Fluids A: Fluid Dynamics*, 3(7):1760–1765, 1991.
- [51] Douglas K Lilly. A proposed modification of the Germano subgrid-scale closure method. *Physics of Fluids A: Fluid Dynamics*, 4(3):633–635, 1992.
- [52] Joseph Smagorinsky. General circulation experiments with the primitive equations: I. The basic experiment. *Monthly Weather Review*, 91(3):99–164, 1963.
- [53] Cecil E. Leith. Diffusion approximation for two-dimensional turbulence. *The Physics of Fluids*, 11(3):671–672, 1968.
- [54] CE Leith. Stochastic models of chaotic systems. *Physica D: Nonlinear Phenomena*, 98(2-4):481–491, 1996.
- [55] Stephen B Pope. *Turbulent Flows*. IOP Publishing, 2001.
- [56] Charles Meneveau and Joseph Katz. Scale-invariance and turbulence models for large-eddy simulation. *Annual Review of Fluid Mechanics*, 32(1):1–32, 2000.
- [57] Guido Boffetta and Robert E Ecke. Two-dimensional turbulence. *Annual Review of Fluid Mechanics*, 44:427–451, 2012.
- [58] Pavel A Perezhogin. 2D turbulence closures for the barotropic jet instability simulation. *Russian Journal of Numerical Analysis and Mathematical Modelling*, 35(1):21–35, 2020.
- [59] Yifei Guan, Adam Subel, Ashesh Chattopadhyay, and Pedram Hassanzadeh. Learning physics-constrained subgrid-scale closures in the small-data regime for stable and accurate LES. *Physica D: Nonlinear Phenomena*, 443:133568, 2023.
- [60] Geoffrey K Vallis. *Atmospheric and Oceanic Fluid Dynamics*. Cambridge University Press, 2017.
- [61] Yifei Guan, Adam Subel, Ashesh Chattopadhyay, and Pedram Hassanzadeh. Learning physics-constrained subgrid-scale closures in the small-data regime for stable and accurate LES. *Physica D: Nonlinear Phenomena*, 443:133568, 2023.
- [62] Lothar Heimbach, Sebastian Kaltenbach, Petr Karnakov, Francis J Alexander, and Petros Koumoutsakos. Reinforcement learning closures for underresolved partial differential equations using synthetic data. *Computer Methods in Applied Mechanics and Engineering*, 452:118767, 2026.
- [63] Gary J Chandler and Rich R Kerswell. Invariant recurrent solutions embedded in a turbulent two-dimensional Kolmogorov flow. *Journal of Fluid Mechanics*, 722:554–595, 2013.
- [64] Dmitrii Kochkov, Jamie A Smith, Ayya Alieva, Qing Wang, Michael P Brenner, and Stephan Hoyer. Machine learning–accelerated computational fluid dynamics. *Proceedings of the National Academy of Sciences*, 118(21), 2021.
- [65] Julia Ling, Andrew Kurzawski, and Jeremy Templeton. Reynolds averaged turbulence modelling using deep neural networks with embedded invariance. *Journal of Fluid Mechanics*, 807:155–166, 2016.

- [66] Guido Novati and Petros Koumoutsakos. Remember and forget for experience replay. In Kamalika Chaudhuri and Ruslan Salakhutdinov, editors, *Proceedings of the 36th International Conference on Machine Learning*, volume 97 of *Proceedings of Machine Learning Research*, pages 4851–4860. PMLR, 09–15 Jun 2019.
- [67] Pascal Weber, Daniel Wälchli, Mustafa Zeqiri, and Petros Koumoutsakos. Remember and forget experience replay for multi-agent reinforcement learning. *arXiv preprint arXiv:2203.13319*, 2022.
- [68] Sergio M. Martin, Daniel Wälchli, Georgios Arampatzis, Athena E. Economides, Petr Karnakov, and Petros Koumoutsakos. Koral: Efficient and scalable software framework for bayesian uncertainty quantification and stochastic optimization. *Computer Methods in Applied Mechanics and Engineering*, 389:114264, 2022.
- [69] Hugo Frezat, Guillaume Balarac, Julien Le Sommer, Ronan Fablet, and Redouane Lguensat. Physical invariance in neural networks for subgrid-scale scalar flux modeling. *Physical Review Fluids*, 6(2):024607, 2021.
- [70] Tim Woollings, David Barriopedro, John Methven, Seok-Woo Son, Olivia Martius, Ben Harvey, Jana Sillmann, Anthony R Lupo, and Sonia Seneviratne. Blocking and its response to climate change. *Current climate change reports*, 4:287–300, 2018.
- [71] Takuya Iwanaga, William Usher, and Jonathan Herman. Toward salib 2.0: Advancing the accessibility and interpretability of global sensitivity analyses. *Socio-Environmental Systems Modelling*, 4:18155–18155, 2022.
- [72] Yifei Guan and Pedram Hassanzadeh. Semi-analytical eddy-viscosity and backscattering closures for 2d geophysical turbulence. *arXiv preprint arXiv:2504.09670*, 2025.

## A A-posteriori analysis in turbulent kinetic energy spectra

In this section, we compare the turbulent kinetic energy spectra,  $\hat{E}(k)$ , of the LES with SMARL-based (RL-Smag and RL-Leith) and traditional dynamic Smag and Leith (DSmag and DLeith) models with the ones obtained from DNS. The SMARL-based models match the DNS/FDNS spectra over the whole spectrum  $k \in [0, k_c]$  across all 4 cases, outperforming both the DSmag and DLeith models.

## B Sensitivity analysis of the policy

In this section, we investigate which states are responsible for the most change in the output of the policy. To do so, we train the RL agents in cases 1, 2, 3, and 4 (see Section 5.5) with both the Smagorinsky and Leith models. The input states contain the five nonzero local invariants of the velocity gradient and velocity Hessian, followed by the logarithm of the enstrophy spectrum. We then compute the first-order Sobol indices of the policy for each input state, using the SALib package [71].

Fig. 7 shows the first-order Sobol indices for all three cases with the RL-Leith and RL-Smagorinsky models, respectively. We observe that in all cases, the first five states, corresponding to the local invariants of the velocity gradient (2 local invariants in 2D turbulence) and velocity Hessian (3 local invariants in 2D turbulence) [41], have a nearly zero first-order Sobol index. This means that the policy does not depend on these states, and we have thus chosen to remove them from the input of the policies in this study. We also note that in most cases, input states that correspond to low frequencies of the enstrophy spectrum have a dominant first-order Sobol index, indicating that high frequencies do not play a major role in the control of the coefficients  $c_s$  and  $c_l$ .

The effects of local states on the *a-posteriori* results are shown in Fig. 8. In terms of predicting the probability density function of vorticity,  $\mathcal{P}(\omega)$ , the RL models with local states perform similarly to those

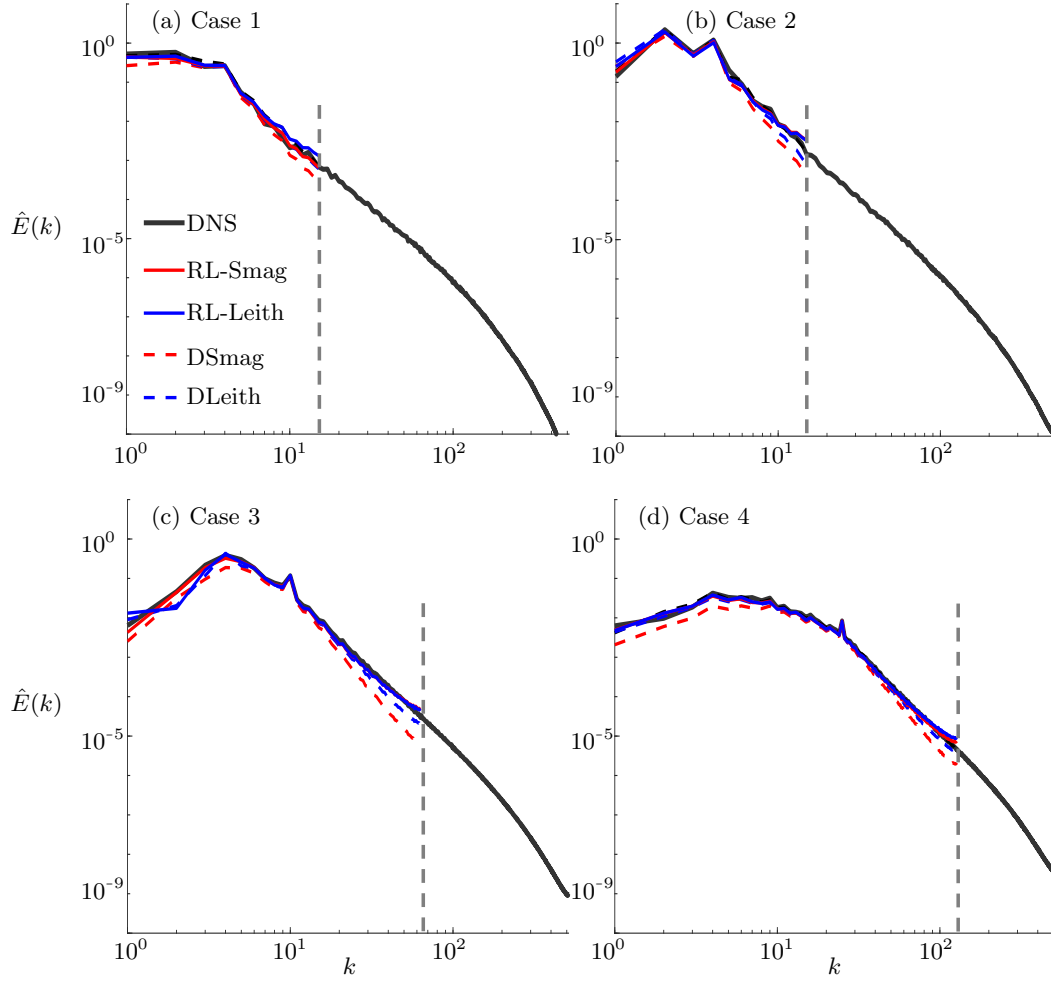


Figure 6: *A-posteriori* testing results in terms of turbulent kinetic energy spectra,  $\hat{E}(k)$ . The gray dash lines mark the cut-off wavenumber,  $k_c$ . The FDNS spectra is the same as the DNS spectra up to  $k_c$ .

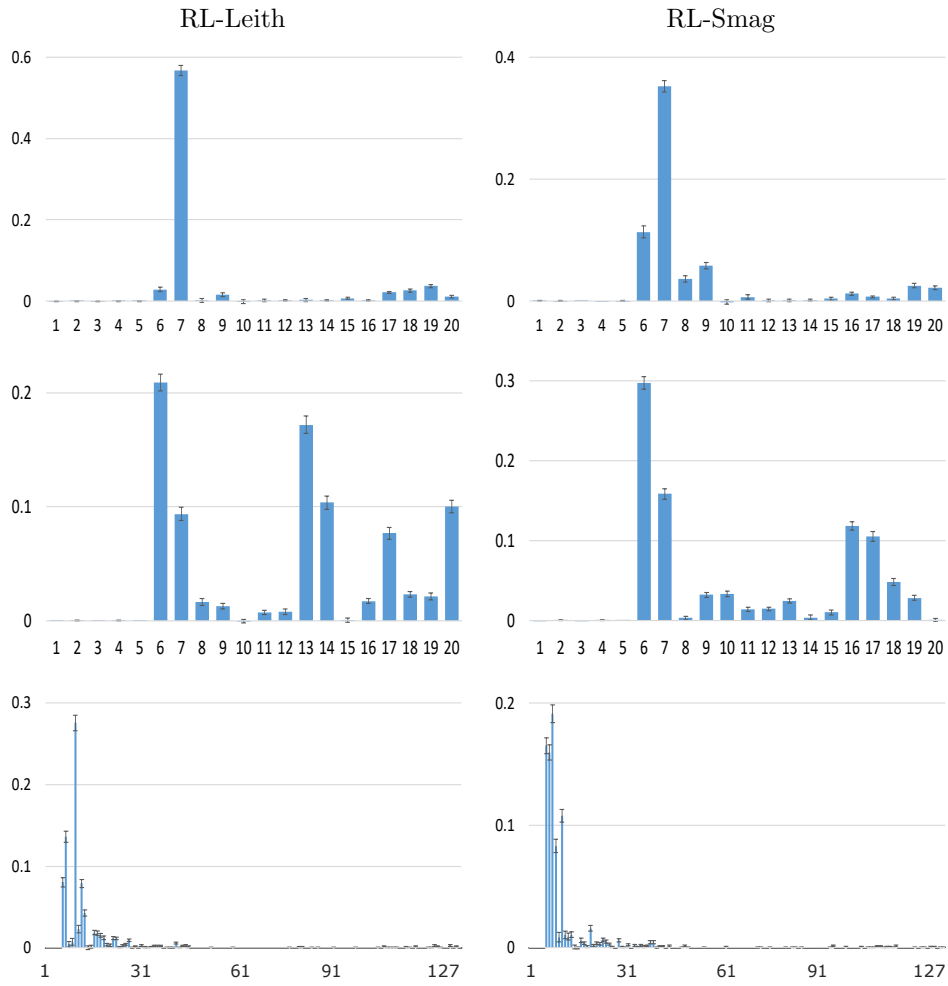


Figure 7: First-order Sobol indices of the policies trained with RL-Leith and RL-Smag for all (local + global) states in Cases 1, 2, and 4 (from top to bottom).

with global states only (see Fig. 2). Another note is that Smag and Leith perform similarly with RL optimized coefficients, which is reasonable due to the equivalence of both models in 2D once their coefficients are optimized [40, 72].

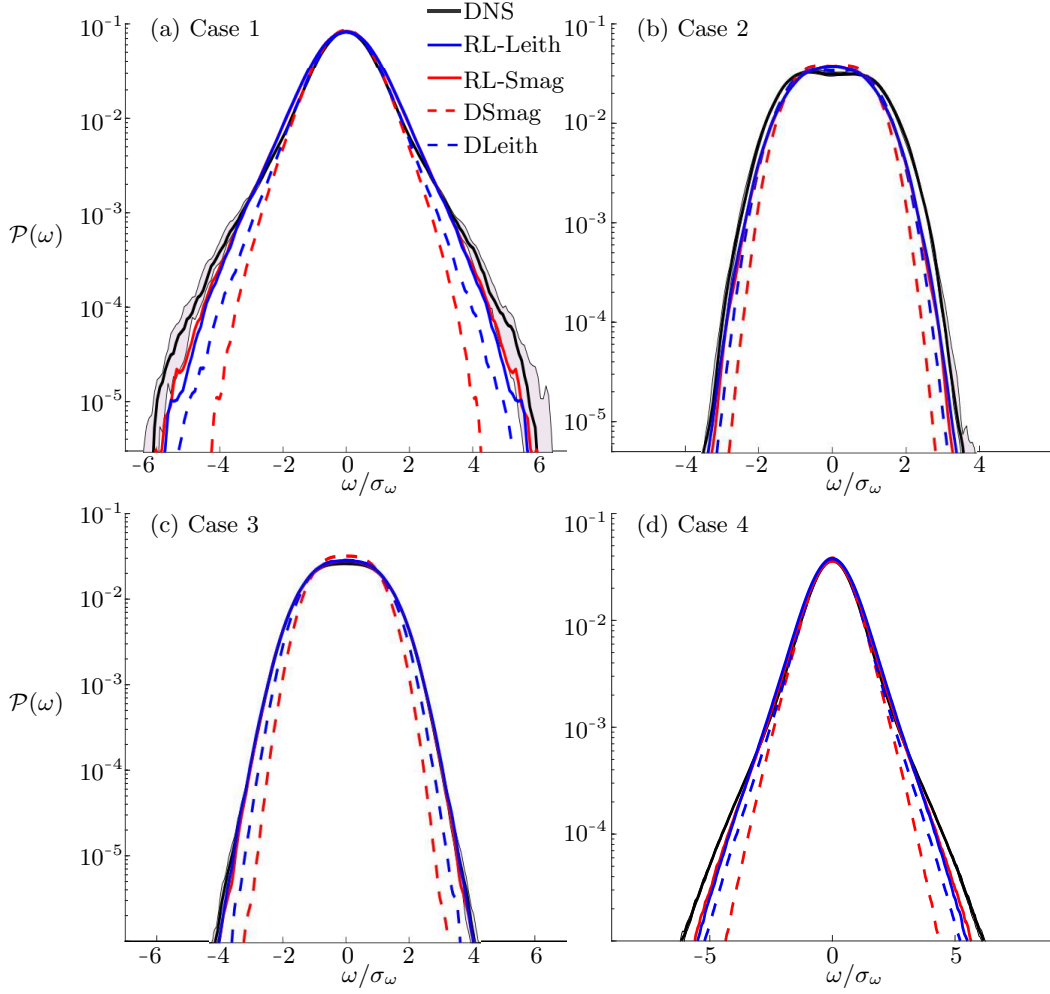


Figure 8: *A-posteriori* testing results in terms of probability density function of vorticity ( $\mathcal{P}(\omega)$ ). The  $x$ -axis is normalized by the standard deviation of vorticity ( $\sigma_\omega$ ) computed from DNS of each case. The shading area represents the uncertainty (25-75 quartiles) of the DNS PDF. Here, the RL models take both local states (5 invariants of velocity gradient and velocity Hessian tensors) and global states (logarithm of enstrophy spectrum) as inputs.